European Heart Journal – Cardiovascular Imaging (2016) **17**, 877–884
doi:10.1093/ehjci/jev228

Four-dimensional flow magnetic resonance imaging-based characterization of aortic morphometry and haemodynamics: impact of age, aortic diameter, and valve morphology

Julio Garcia[1], Alex J. Barker[1], Ian Murphy[1], Kelly Jarvis[1,2], Susanne Schnell[1], Jeremy D. Collins[1], James C. Carr[1], S. Chris Malaisrie[3], and Michael Markl[1,2]*

[1]Department of Radiology, Northwestern University, 737 N Michigan, Suite 1600, Chicago, IL 60611, USA; [2]Biomedical Engineering, Northwestern University, Evanston, IL, USA; and [3]Division of Cardiothoracic Surgery, Northwestern University, Chicago, IL, USA

Received 31 July 2015; accepted after revision 21 August 2015; online publish-ahead-of-print 15 September 2015

Aims Four-dimensional (4D) flow magnetic resonance imaging (MRI) was employed for the simultaneous assessment of morphometry and flow parameters along the thoracic aorta to investigate associations between flow, age, aorta diameter, and aortic valve morphology.

Methods and results One hundred and sixty-five subjects, 65 controls, 50 patients with bicuspid aortic valve (BAV), and 50 patients with a dilated aorta, and a tricuspid aortic valve (TAV) underwent 4D flow MRI. Following 3D segmentation of the aorta, a vessel centreline was calculated and used to extract aorta diameter, peak systolic velocity, and normalized systolic flow displacement. Validation of 4D flow MRI-based morphometric measurements compared with manual diameter measurements from standard contrast-enhanced MR angiography in 20 controls showed good agreement (mean difference = 0.4 mm, limits of agreement = $\pm$ 1.31 mm) except at the sinus of valsalva. BAV showed significant differences in average peak velocity (PV; $P < 0.016$) compared with TAV and controls between the left ventricle outflow tract to sino-tubular junction (BAV: 1.3 $\pm$ 0.3 m/s; TAV: 1.2 $\pm$ 0.2 m/s; controls: 1.0 $\pm$ 0.1 m/s) and the ascending aorta for average normalized flow displacement (BAV: 0.11 $\pm$ 0.02; TAV: 0.09 $\pm$ 0.02; controls: 0.06 $\pm$ 0.01, $P < 0.016$) despite similar average aortic dimensions for BAV (37 $\pm$ 1 mm) and TAV (39 $\pm$ 1 mm). Multivariate linear regression showed a significant correlation of maximal aortic diameter to age, PV, and normalized flow displacement ($R^2 = 0.413$, $P < 0.001$).

Conclusion A single acquisition of 4D flow MRI characterized local morphological and haemodynamic differences between groups along the aorta. BAV showed altered haemodynamics when compared with TAV in spite of having similar aorta dimensions. Maximal aorta diameter was associated with age, PV, and normalized flow displacement.

Keywords Aortic diseases • Haemodynamics • Magnetic resonance imaging

Introduction

There is considerable debate regarding the possible mechanisms responsible for aortic dilatation in patients with tricuspid aortic valve (TAV) and bicuspid aortic valve (BAV).[1] In addition to a suspected genetic component, there is increasing evidence that three-dimensional (3D) flow pattern alterations in the ascending aorta are common in BAV patients and possibly related to the development of aortopathy.[2,3] However, aortic morphometry and flow parameters are separately measured in standard imaging protocols at specific anatomic landmarks.[4,5] For example, aortic morphometry is typically assessed by echocardiography, computed tomography angiography, or magnetic resonance angiography (MRA),[4] while flow parameters are assessed by echocardiography or two-dimensional (2D) flow

* Corresponding author. Tel: +1 312 694 7780; Fax: +1 312 926 5991. *E-mail address*: mmarkl@northwestern.edu

magnetic resonance imaging (MRI).[5] However, anatomic landmarks and 2D planar reformatting are subject to observer variability and lead to regional variations when measuring aortic size, the actual location of peak velocity (PV),[6–8] and normalized flow displacement.[9] In this regard, the simultaneous assessment of aortic morphometry and flow parameters may improve the monitoring of disease progression and clinical management.

Advanced four-dimensional (4D) flow MRI allows for the assessment of 3D blood flow velocity with full volumetric coverage of the thoracic aorta,[10] and can be used to calculate 3D phase-contrast angiograms (PC-MRA) to provide information on aortic size and geometry. Therefore, the purpose of this study was to apply 4D flow MRI for the simultaneous semi-automatic assessment of aorta morphometry and flow parameters along the entire volume of the thoracic aorta. The aim was to test the hypotheses that: (i) a 3D PC-MRA computed from the 4D flow MRI exam can detect differences in aortic dimensions and haemodynamics throughout the entire aorta in a single acquisition; (ii) BAV morphology will significantly impact haemodynamic parameters compared with TAV patients with aortic dilatation; and (iii) changes in aortic dimensions are associated with age and flow parameters.

Methods

Study population

An existing database of 199 subjects was queried to identify candidates for study inclusion. A total of 165 subjects [65 healthy controls (age = 43 ± 14 years, 25 females), 50 BAV patients (age = 49 ± 14 years, 12 females), and 50 TAV patients (age = 61 ± 14 years, 9 females) with a dilated ascending aorta] were included in the study. Patients were enrolled using an IRB-approved retrospective chart review for those who underwent a standard-of-care MRI between February and August 2014 for surveillance of aorta size. Patients were excluded if the data were incomplete (4D flow data incomplete; $n = 4/69$ controls) or if the 3D PC-MRA was not calculated for further analysis at time when data were collected (i.e. 3D segmentation cannot be perform, $n = 12/62$ for BAV and $n = 8/68$ for TAV). BAV cases were identified using the Sievers's classification: BAV type 0 (no raphe) anteroposterior and lateral, BAV type 1 (one raphe) with RL fusion pattern (raphe between left coronary and right coronary sinuses) and RN fusion pattern (raphe between right coronary and non-coronary sinuses), and BAV type 2/unicuspid (two raphes) with RL/RN fusion patterns.[11] All volunteers underwent 4D flow MRI based on an IRB-approved protocol and informed consent was obtained.

Magnetic resonance imaging

MRI was performed on 1.5 T ($n = 119$) and 3 T ($n = 46$) systems (Magnetom Aera and Skyra, Siemens AG, Erlangen, Germany). All subjects underwent standard-of-care CMR of the thorax, including dynamic 2D cine steady state free precession imaging of the heart and aortic valve. Research 4D flow MRI was acquired in a sagittal oblique 3D volume covering the thoracic aorta with prospective ECG-gating and a respiratory navigator placed on the lung–liver interface.[10] Pulse sequence parameters were as follows: flip angle = 15°, spatial resolution = 1.66–2.81 × 1.66–2.81 × 2.2–3.7 mm^3, temporal resolution = 36.8–43.2 ms. Velocity encoding was adjusted to minimize velocity aliasing (1.5–4.0 m/s) based on the three-chamber view of in-plane standard 2D PC MRI scout images. 4D flow MRI acquisition times varied from 8 to 15 min. In 20 controls, the streamlined 3D PC-MRA morphometry measurements were validated against the guideline recommendations for manual measurement of aorta dimensions[4] using a standard-of-care contrast-enhanced MRA (CE-MRA) (Magnevist, Ablavar, Multihance) using ECG-gated 3D fast low angle shot sequence (FLASH, FOV = 384 × 192–240, resolution = 1.17–1.30 × 1.17–1.30 × 1.4–1.8 mm^3, flip angle = 30°).[12]

Novel 4D flow data analysis

All 4D flow MRI data were corrected for eddy currents, Maxwell terms, and velocity aliasing using Matlab (Mathworks, Natick, MA, USA).[13] The 3D PC-MRA was computed for each subject using the pre-processed 4D flow MRI data as given by $I_i^{PC\text{-}MRA}(\vec{r}) = I_i^{Mag}(\vec{r})\sqrt{\sum_{j=x,y,z} v_{j,i}^2(\vec{r})}$, where I_i^{Mag} is the magnitude image, $\vec{r}$ is the spatial location within the 3D volume, v is the velocity-encoded image with j representing the velocity encoding direction in image coordinates (x, y, z), and i is the measured time frame within the cardiac cycle.[10] The 3D PC-MRA data were used to manually segment the aortic lumen in 3D (Mimics, Materialise, Leuven, Belgium) (*Figure 1A*).[14] A volume centreline (*Figure 1B*) was

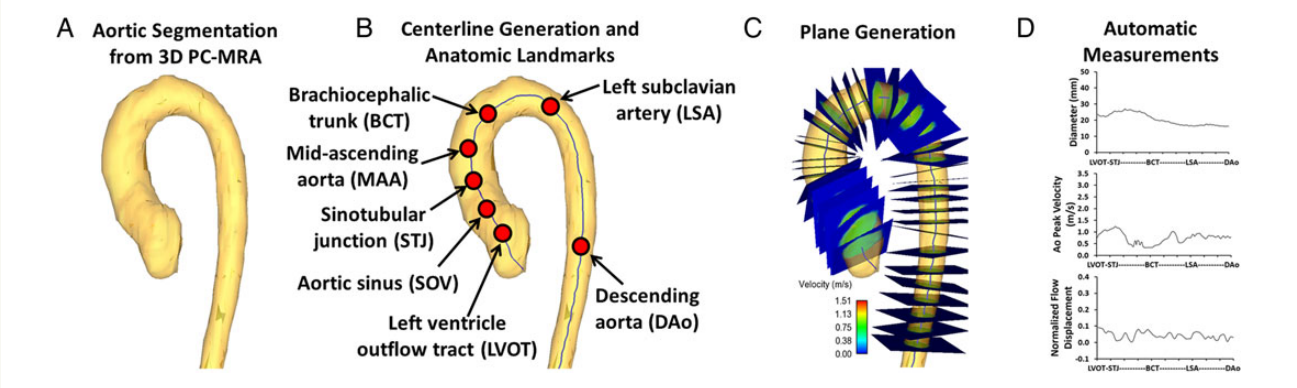

Figure 1 Workflow for aortic diameter and flow parameters measurements. (*A*) 3D PC-MRA, which was used for aorta segmentation. (*B*) Centreline calculation from the segmented volume and the anatomic landmarks definition along the centreline. (*C*) Examples of plane generation along the centreline. The generated planes were used to calculate aorta diameter, PV, and normalized flow displacement as it is shown in (*D*). All measurements were normalized to standard landmarks distance.

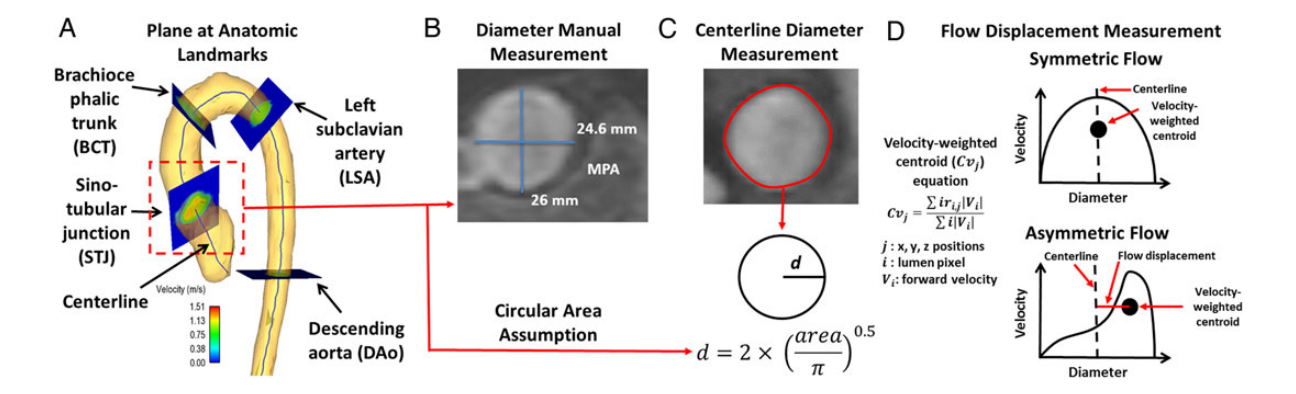

Figure 2 Centreline plane-based measurements. (*A*) Analysis workflow, multiple analysis planes were created along the centreline to measure vessel diameter and flow parameters, anatomic landmark planes are displayed for distance reference. (*B*) Example of manual measurement of diameter using standard CE-MRA, this measurement was performed only in 20 cases for diameter validation and the larger diameter was used for assessment. (*C*) Automatic measurement of diameters obtained from a plane based on the 3D CE-MRA segmentation (red line corresponds to segmented vessel area), note that a circular cross section was assumed to back calculate diameter (*d*). (*D*) Examples of flow displacement measurements for symmetric and asymmetric flow profiles. The black dashed line corresponds to the vessel centreline. The normalized flow displacement was calculated as the distance from the vessel centreline to the positive velocity-weighted centre of mass (black circle) normalized to the vessel diameter. The corresponding equation is also shown in (*D*). MPA, main pulmonary artery.

automatically calculated based on the aorta 3D segmentation[15] (>250 nodes depending on the aorta length and morphometry). The 3D PC MRI dataset was subsequently masked using the 3D segmentation. The mean velocity was calculated over the masked volume along the cardiac cycle and the peak systolic time point was identified at the maximal mean velocity. The centreline nodes were used to automatically create analysis planes perpendicular to the vessel (*Figure 1C*) for the calculation of diameter, normalized flow displacement and PV at the time-point of peak systole. The vessel diameter for each plane was calculated assuming a circular area. Flow displacement was defined as the distance between the vessel centreline node and the forward velocity-weighted centre of mass position and was normalized to the vessel diameter to achieve the normalized flow displacement (*Figure 2D*).[2,9] The PV was extracted using the velocity-weighted centre of mass location to avoid a single velocity voxel measurement.

Standardized anatomic landmarks [left ventricle outflow tract (LVOT), aortic sinus (SOV), sino-tubular junction (STJ), mid-ascending aorta (MAA), brachiocephalic trunk (BCT), left subclavian artery, and descending aorta (Dao), *Figure 1B*] were manually identified in each case and used to normalize the measurements along the aorta centreline distance (*Figure 1D*). Aortic valve stenosis (PV) and regurgitation severity (regurgitant fraction) were measured at the STJ plane and ranged between mild (2.0–2.9 m/s), moderate (3.0–3.9 m/s), and severe (>4.0 m/s).[5] Aortic valve effective orifice area was calculated using the jet shear layer detection method.[8,16,17]

The streamlined morphometry assessment strategy (3D segmentation, centreline generation, extraction of aortic diameters along centreline) was validated in 20 controls in three steps: (i) by comparing the automated centreline diameter (obtained from the 3D segmentation of the CE-MRA) with manual diameter measurements of the same CE-MRA at the anatomic landmarks using dedicated multi-planar software (Vitrea Enterprise Suite 6.6.3, Toshiba Medical, Rolling Meadows, IL, USA); (ii) by comparing automated 3D PC-MRA-based morphometry assessment with manually measured diameters at anatomic landmarks obtained from the clinical reference standard CE-MRA; (iii) by comparing automated 3D PC-MRA-based morphometry assessment with automated 3D CE-MRA-based morphometry.

Statistical analyses

All continuous data are presented as mean ± standard deviation. A Shapiro–Wilk test was used to evaluate normal distribution of measured parameters. The agreement between standard CE-MRA, CE-MRA, and 4D flow MRA was assessed by Bland–Altman analysis, and the mean difference and limits of agreement (± 1.96 SD) were calculated. The average difference (in %) between methods was calculated. To compare aorta diameters and haemodynamic parameters between healthy controls, BAV, and TAV, a one-way analysis of variance (Gaussian distribution) or Kruskal–Wallis (non-Gaussian distribution) was performed. If these tests determined that a parameter was significantly different between groups ($P < 0.05$), multiple comparisons for all groups were performed using an independent-sample *t*-test (Gaussian distribution) or Mann–Whitney test (non-Gaussian distribution). Bonferroni correction was used to adjust for multiple comparisons and the differences were considered significant if $P < 0.0166$. Associations between aortic dimensions with age and flow parameters were assessed by Pearson's correlation. A correlation was considered significant for $P < 0.001$ and $R > 0.4$.[18] A multivariate linear regression was performed including significant Pearson's correlations and adjusted by age. Statistical analysis was performed using SPSS 17 (SPSS, Chicago, IL, USA).

Results

Study cohort

The demographics of the study cohort are summarized in *Table 1*. Patients with TAV were significantly ($P < 0.001$) older than patients with BAV. Left ventricular stroke volume was higher in BAV patients than TAV (100 ± 24 vs. 91 ± 26 mL, $P = 0.007$). Valve effective orifice area was significantly smaller in BAV than TAV (2.0 ± 0.7 vs. 2.5 ± 0.8 cm^2, $P = 0.001$). The distribution of BAV fusion

Table 1 Patient characteristics

	Controls	BAV	TAV	P-value Controls vs. BAV	P-value Controls vs. TAV	P-value TAV vs. BAV	P-value overall
n	65	50	50				
Age (years)	43 ± 14 (78, 19)	49 ± 14 (80, 23)	61 ± 14 (85, 26)	0.017	<0.001	<0.001	<0.001
Female	25 (38%)	12 (24%)	9 (18%)	0.101	0.018	0.464	0.041
Height (m)	1.72 ± 0.08 (1.90, 1.52)	1.77 ± 0.08 (1.96, 1.55)	1.61 ± 0.19 (1.93, 1.27)	0.002	0.017	<0.001	<0.001
Weight (kg)	84 ± 19 (136, 54)	83 ± 13 (123, 59)	86 ± 17 (140, 43)	–	–	–	0.561
Effective orifice area (cm^2)	2.6 ± 0.5 (1.8, 4.0)	2.0 ± 0.7 (0.9, 3.5)	2.5 ± 0.8 (0.9, 3.9)	<0.001	0.65	0.001	<0.001
Stenosis severity							
Mild	0 (0%)	14 (28%)	7 (14%)	<0.001	0.002	0.087	<0.001
Moderate	0 (0%)	3 (6%)	0 (0%)	0.046	–	0.08	0.03
Severe	0 (0%)	0 (0%)	0 (0%)	–	–	–	–
Regurgitation severity							
Mild	0 (0%)	6 (12%)	4 (8%)	0.004	0.021	0.5	0.023
Moderate	0 (0%)	4 (8%)	7 (14%)	0.021	0.002	0.34	0.011
Severe	0 (0%)	1 (2%)	1 (2%)	–	–	–	0.317

All continuous data are presented as mean ± standard deviation (max, min) or number (%). *P*-value resulted from independent-sample *t*-test (Gaussian distribution) or Mann–Whitney (non-Gaussian distribution) comparing subjects groups.
BAV, bicuspid aortic valve; TAV, tricuspid aortic valve.

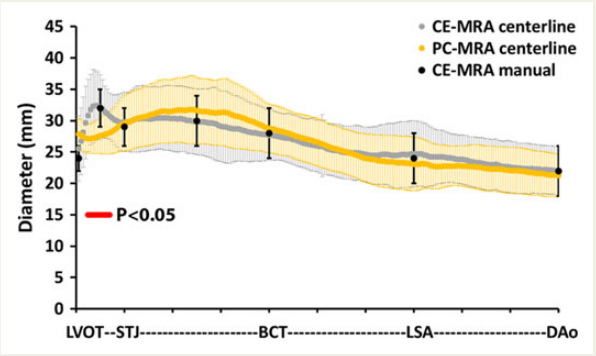

Figure 3 Validation of aorta diameter measurement based on centreline planes. Aorta diameter determined by three different methods: (i) manual measurements based on standard multi-planar CE-MRA (black dots and bars representing mean and standard deviation), (ii) centreline-based automatic diameter detection using PC-MRA (yellow dots and bars representing mean and standard deviation), and (iii) centreline-based automatic diameter detection using CE-MRA (grey dots and bars representing mean and standard deviation) for 20 subjects were used to validate centreline-based diameters. Red dots indicate significant differences ($P < 0.05$, independent-sample *t*-test) between centreline-based CE-MRA and PC-MRA diameters.

patterns was as follows: type 1 RL ($n = 30$), type 1 RN ($n = 10$), BAV type 0 ($n = 4$), and BAV type 2 ($n = 6$). Aortic stenosis severity was mild ($n = 14$) and moderate ($n = 3$) in 34% of BAV, and mild ($n = 7$) in 14% of TAV. Aortic regurgitation was present in ($n = 12$) 24% of BAV patients and in ($n = 11$) 22% of TAV.

Validation of aortic diameter measurement

Data processing and segmentation of 3D PC-MRA required 10–20 min for each subject. As demonstrated by Bland–Altman analysis (mean difference = 0.4 mm, limits of agreement = ± 1.31 mm, average difference = 2 ± 2%), aortic dimensions at anatomic landmarks obtained by the clinical reference standard (i.e. manual measurements based on 3D CE-MRA) were similar compared with the 3D CE-MRA centreline-based calculations (*Figure 3*, *Table 2*). Similarly, the clinical reference standard demonstrated good agreement with 3D PC-MRA centreline-based calculation (mean difference = 0.12 mm, limits of agreement = ± 5 mm, average difference = 7 ± 6%, *Table 2*). Furthermore, 3D CE-MRA-based diameters along the entire aorta were similar compared with 4D flow MRI-derived dimensions with good agreement between both techniques (mean difference = 0.11 mm, limits of agreement = ± 2.22 mm, average difference = 4 ± 3%, *Table 2*). Significantly lower diameters were found at the SOV between 3D PC-MRA-derived diameters and 3D CE-MRA (28 ± 3 vs. 32 ± 5 mm, $P < 0.05$, *Table 2*).

Differences in aortic diameter and flow parameters

Figure 4 depicts the distribution of aortic diameter (*Figure 4A*), PV (*Figure 4B*), and normalized flow displacement (*Figure 4C*) along

Table 2 Validation of aortic diameter measurements

Standardized anatomic landmarks	Manual diameter from 3D CE-MRA (mm)	Centreline diameter from 3D CE-MRA (mm)	Centreline diameter from 3D PC-MRA (mm)
Left ventricle outflow tract	24 ± 2	26 ± 5	28 ± 2
Aortic sinus	32 ± 3	32 ± 5	28 ± 3†
Sino-tubular junction	29 ± 3	30 ± 5	30 ± 4
Mid-ascending aorta	30 ± 4	30 ± 5	32 ± 5
Brachiocephalic trunk	28 ± 4	28 ± 4	29 ± 4
Left subclavian artery	24 ± 4	25 ± 5	23 ± 4
Descending aorta	22 ± 4	22 ± 4	21 ± 3

All continuous data are presented as mean ± standard deviation.
†$P < 0.05$, *P*-value resulted from independent-sample *t*-test comparing centreline diameter from 3D PC-MRA vs. manual/centreline diameter from 3D CE-MRA diameter.

the aorta, normalized to the anatomic landmarks and averaged for each cohort. The average aorta diameter in the ascending aorta, from STJ to BCT, was significantly higher for BAV vs. control (37 ± 1 vs. 30 ± 1 mm, $P < 0.0166$), and for TAV vs. controls (39 ± 1 vs. 30 ± 1 mm, $P < 0.0166$). The maximal aorta diameter was significantly higher in the ascending aorta, from STJ to BCT, for BAV vs. controls (39 ± 6 vs. 31 ± 5 mm, $P < 0.0166$) and TAV vs. controls (40 ± 6 vs. 31 ± 5 mm, $P < 0.0166$). The maximal PV value along the centreline was located within the LVOT–STJ section (1.1 ± 0.3 m/s for controls, 1.4 ± 0.5 m/s for TAV, and 1.6 ± 0.6 m/s for BAV, $P < 0.0166$ between all groups, *Figure 4B*). The average PV in the LVOT to STJ section was significantly higher for BAV vs. control (1.3 ± 0.3 vs. 1.0 ± 0.1 m/s, $P < 0.0166$), for TAV vs. controls (1.2 ± 0.2 vs. 1.0 ± 0.1 m/s, $P < 0.0166$), and for BAV vs. TAV (1.3 ± 0.3 vs. 1.2 ± 0.2 m/s, $P < 0.016$). In particular, four BAV and one TAV cases presented discordances between valve effective orifice area and PV. The average normalized flow displacement (*Figure 4C*) from the STJ to BCT was significantly higher for BAV vs. controls (0.11 ± 0.02 vs. 0.06 ± 0.01, $P < 0.016$), for TAV vs. controls (0.09 ± 0.02 vs. 0.06 ± 0.01, $P < 0.016$), and for BAV vs. TAV (0.10 ± 0.02 vs. 0.09 ± 0.02, $P < 0.016$). In addition, the maximal normalized flow displacement was 75% higher in BAV subjects and 85% higher in TAV subjects, when compared with control subjects ($P < 0.016$).

Valve morphology impact on aortic dimensions and haemodynamic patterns

The average aorta diameter was significantly larger in TAV patients compared with BAV patients in the aortic arch (30 ± 5 vs. 28 ± 4 mm, $P < 0.016$) and in the DAo (26 ± 1 vs. 23 ± 1 mm, $P < 0.016$, *Figure 4A*). Also, the averaged normalized flow displacement was significantly higher in BAV patients compared with TAV patients (0.09 ± 0.01 vs. 0.07 ± 0.01, $P < 0.016$) at the STJ section. The BAV patient group with RL valve morphology showed a slightly bigger maximal aortic diameter (37 ± 4 vs. 36 ± 6 mm) and PV (1.65 ± 0.63 vs. 1.53 ± 0.46 m/s) than the patients with RN morphology, as well as smaller maximal normalized flow displacement (0.11 ± 0.05 vs. 0.13 ± 0.07); however, no significant differences were found.

Aortic diameter associations with age and flow parameters

Significant correlations of maximal aorta diameter with age ($r = 0.52$, $P < 0.001$) and PV ($r = 0.44$, $P < 0.001$) could be detected (*Table 3*). However, the correlations were mainly driven by the control group for age ($r = 0.55$, $P < 0.001$) and PV ($r = 0.45$, $P < 0.001$). Multivariate linear analysis ($R^2 = 0.6$, $P < 0.001$, *Table 3*) shows that age and PV are correlated with maximal aortic diameter size as adjusted by age.

Discussion

The main findings of this study were: (i) the presence of BAV significantly impacted flow haemodynamic parameters, while ascending aorta diameter between the BAV and TAV patient groups was similar; (ii) morphometric and haemodynamic differences in the aorta can be detected using a single 4D flow MRI acquisition of the entire aorta, except at the SOV; (iii) the maximum aorta diameter showed a multifactorial association with age, PV, and normalized flow displacement.

PC-MRA diameter validation and centreline measurements

An important component of this study was the cross-validation of 3D PC-MRA with 3D CE-MRA and the use of standard-of-care measurements made using multi-planar CE-MRA reconstruction. Previously, Bock *et al.*[19] showed that the agreement of 3D PC-MRA with CE-MRA improves with the use of contrast agent during acquisition, and Strecker *et al.*[20] demonstrated that scanner strength does not affect derived 4D flow MRI calculations. This comparison was performed using manual placement of single plane measurements in the ascending aorta, aortic arch, and DAo. In the current study, we found good agreement between 3D PC-MRA and CE-MRA using the volumetric centreline method to automatically place multiple analysis planes. The 3D PC-MRA centreline approach avoids the time consuming process of manually aligning the measurement planes by creating regularly spaced measurement slices, which are automatically aligned orthogonal to the vessel of interest. User interaction was reduced to involve only choosing the anatomic

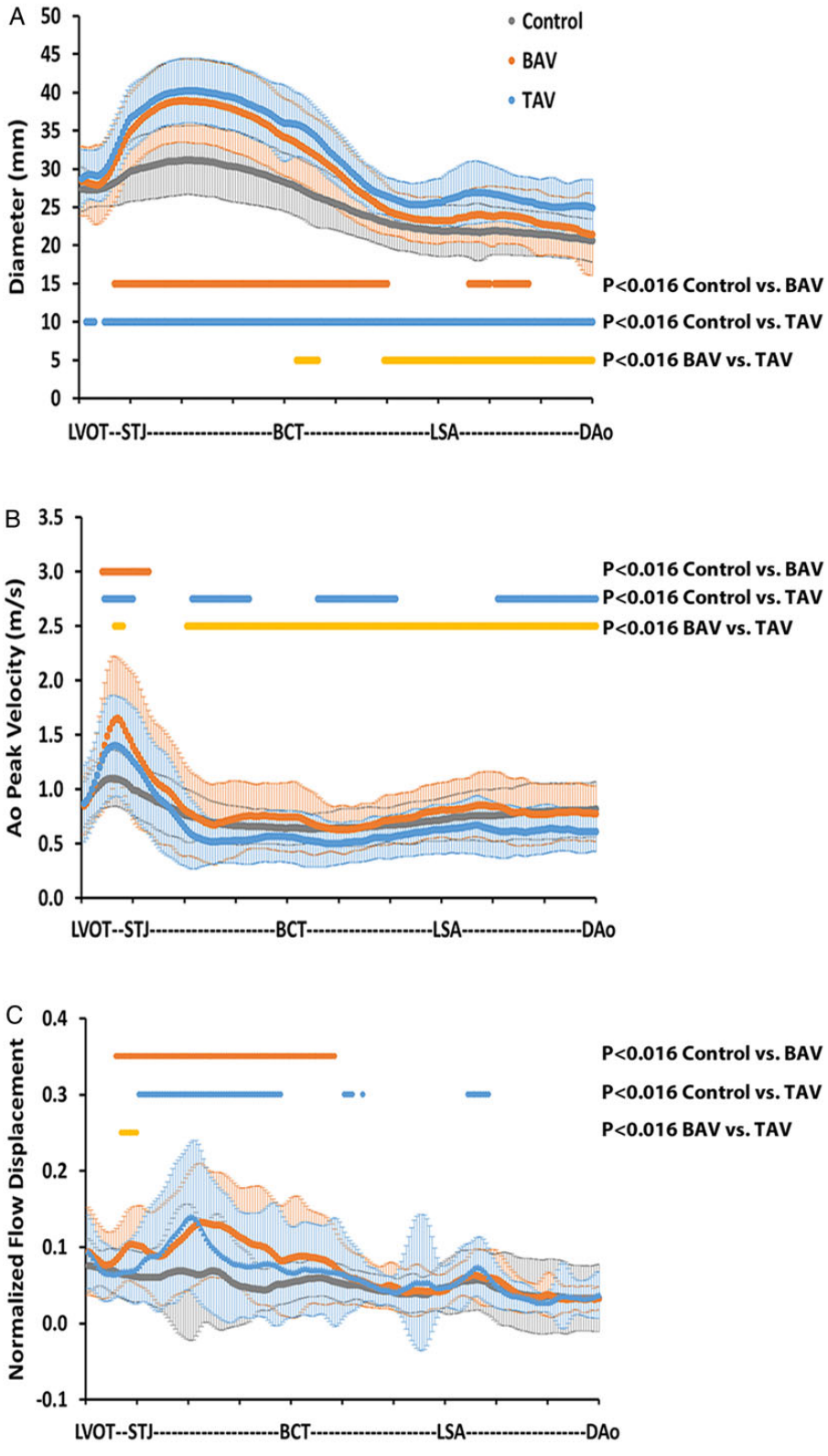

Figure 4 Morphometric and haemodynamic measurements in the entire aorta. (*A*) Aorta diameter for healthy controls (grey dots and bars for mean and standard deviation), patients with BAV (orange dots and bars for mean and standard deviation) and TAV patients (blue dots and bars for mean and standard deviation). (*B*) PV for controls, patients with BAV and TAV. (*C*) Normalized flow displacement for controls, patients with BAV and TAV. Orange dots indicate significant differences between controls and BAV patients. Blue dots indicate significant differences between controls and TAV patients. Yellow dots indicate significant differences between BAV and TAV patients. $P < 0.016$, after Bonferroni correction.

Table 3 Univariate and multivariate determinants of maximal aortic diameter over all groups

	Univariate		Multivariate	
	Std β coefficient ± SE	*P*-value	Std β coefficient ± SE	*P*-value
Age (years)	0.52 ± 0.03	<0.001	0.43 ± 0.07	<0.001
PV (m/s)	0.44 ± 0.79	<0.001	0.33 ± 0.07	<0.001
Normalized flow displacement	0.36 ± 4.83	<0.001	–	–

Std β coeff ± SE: standardized beta coefficient and standard error. $P < 0.001$ and $R > 0.4$ in the univariate models were the criterion for entry of the variable into the multivariate model. The multivariable model overall adjusted $R^2 = 0.6$, $P < 0.001$.

landmark locations, but a map of the parameter of interest can also be produced at a user defined intervals along the vessel centreline (*Figure 1D*). In contrast, most existing studies have evaluated volumetric MRA or 4D flow MRI data by multi-planar reconstruction or the manual positioning of multiple 2D analysis planes along the vessel of interest.[6,21,22]

Compared with the gold standard (manual CE-MRA diameter measurements), we found that the approach presented here was accurate at all landmark positions except at the SOV. We hypothesize that the poor performance of the SOV measurements is due to recirculating blood and low blood velocities in the sinus bulb region as well as the aortic valve motion during the cardiac cycle reducing the PC-MRA contrast. This causes intravoxel dephasing, low signal-to-noise ratio, and ultimately a low PC-MRA signal, which degrades the ability to perform 3D segmentation and extract morphometric information. Future studies may consider using an alternative approach to compute the PC-MRA, such as using the complex difference signal.[23] Nonetheless, we have shown that 4D flow MRI-derived methods can be used to characterize the thoracic aorta beyond the SOV region for BAV and TAV patients with aortic dilatation. Further studies of the proposed strategy are required to resolve measurements in the sinus region.

Size and haemodynamics by cohort

The BAV patient cohort was younger and trended toward having smaller aortic diameters (although not significant) than our TAV patient cohort with aortic dilatations. We suspect these cohort characteristics were confounded by the cross-sectional enrolment approach and the fact that MRI surveillance guidelines for BAV patients dictate more frequent visits.[5]

In our study, PV was located in the proximal aorta (*Figure 4B*) and showed a significant difference ($P < 0.016$) between groups. PV has been previously reported to be located at the vena contracta within the first 5–20 mm from the top leaflets of the aortic valve, depending on the anatomic valve area.[8,24] Since standard 2D flow analysis is generally performed using a single plane at specific locations, the site of PV may not be properly interrogated, resulting in an underestimation of true PV value, particularly with BAV patients due to eccentric flow patterns and/or elevated helical flow.[6,8,14] In this study, no severe aortic stenosis cases were present. While the presence of BAV increased the average PV between the LVOT and STJ (BAV PV = 1.3 ± 0.3 m/s vs. TAV PV = 1.2 ± 0.2 m/s, $P = 0.0166$), the MAA from STJ to BCT were similar, despite diameter differences (BAV max MAA = 37 ± 1 mm vs. TAV max MAA = 39 ± 5 mm, $P = 0.61$).

Normalized flow displacement has been recently proposed as a haemodynamic biomarker in the assessment of BAV patients with aortic dilatation.[2,9,22] Sigovan *et al.*[9] reported that normalized flow displacement was significantly elevated in patients with markedly eccentric and moderate eccentric flow (0.18 ± 0.03 vs. 0.12 ± 0.05, $P < 0.04$). In our study, the control group showed a maximal normalized flow displacement of 0.06 ± 0.08, compared with 0.13 ± 0.08 in BAV group and 0.14 ± 0.09 in TAV group. These results aligned with a moderate normalized flow displacement. In particular, it should be notice that the measurement presented a large variability which may be due to the spread of valve velocities and aortic diameters included in both BAV and TAV groups.

Insights on BAV

Recent studies have demonstrated that the morphologic properties of BAV valves can have abnormal transvalvular flow patterns resulting in a regional increase in wall shear stress.[2,21,25] Given that wall shear stress is known to affect mechanotrasduction pathways associated with vessel wall remodelling, it is worth noting that BAV patients have a higher prevalence and faster rate of ascending aorta dilatation with increased risk of dissection or rupture at younger age compared with TAV patients with dilated ascending aortas.[1,4] In this study, BAV significantly impacted flow haemodynamics in the ascending aorta, as well as aortic diameter. It is possible that the inclusion of flow parameters in the monitoring and management of aortopathy may provide additional insight to this disease.[26] In addition, many efforts have been focused on classification schemes based on histologic features, morphologic valve-fusion patterns, and hierarchical cluster analysis.[11,27–29] The most common valve-fusion patterns involve the right and left cusps with RL fusion pattern, resulting from the fusion in an anterior–posterior leaflet orientation, and RN fusion pattern, resulting from the fusion in a right–left leaflet orientation.[29,30] No significant differences were found between RL and RN groups along the aorta in our study, which may be due to the small cohort size of the RN group ($n = 10$).

Study limitations

A main limitation of this study was related to the PC-MRA 3D segmentation, which required a semi-manual interaction to identify the vessel boundaries, and definition of vessel landmarks. The 3D PC-MRA is partially derived from the sum of the squared velocity

field and weighted by the magnitude images. Thus, the accurate acquisition and pre-processing of the velocity field or magnitude data are necessary to produce a suitable PC-MRA for analysis. In this study, we excluded cases with missing PC-MRA calculation at time of data collection and PC-MRA deemed unsuitable for anatomic measurements. In particular, patients with severe aortic stenosis/regurgitation may be difficult to automatically segment. However, the semi-automatic approach used in this study allowed to correct the 3D segmentation. Even in suitable 3D PC-MRA, we found that the SOV region was poorly resolved. This is due to complex recirculating velocities combined with intravoxel dephasing, which leads to errors in the SOV diameter measurements compared with the CE-MRA. It is important to note that the SOV diameters are an important metric for the assessment of aortic dilatation. In addition, it is important to notice that the validation of 3D PC-MRA aorta morphometry using the standard-of-care 3D CE-MRA did not take into account the wide variation in diameters encountered in patients. As it was mentioned previously, a potential solution may be the use of the complex difference signal to compute the 3D PC-MRA.[23] In clinical practice, the low spatial resolution of MRI acquisition is another important factor.[31] Spatial resolution also affects PV and normalized flow displacement calculation. An additional limitation is the lack of the longitudinal outcome and aortic diameter growth rate.

Conclusion

In conclusion, PV and flow displacement in BAV patients were different from TAV patients, in spite of having similar mid-ascending aorta diameter size. The maximum aorta diameter was also associated with age, PV, and flow displacement. In addition, it has been shown that morphological and haemodynamic measurements can be obtained using a single acquisition of 4D flow MRI.

Conflict of interest: none declared.

Funding

This work was supported by the National Institutes of Health grants R01HL115828, K25HL119608 and American Heart Association grants 14POST18350019 and 14PRE18620016.

References

1. Verma S, Siu SC. Aortic dilatation in patients with bicuspid aortic valve. *N Engl J Med* 2014;**370**:1920–9.
2. Mahadevia R, Barker AJ, Schnell S, Entezari P, Kansal P, Fedak PW *et al.* Bicuspid aortic cusp fusion morphology alters aortic 3D outflow patterns, wall shear stress and expression of aortopathy. *Circulation* 2014;**129**:673–82.
3. Bissell MM, Hess AT, Biasiolli L, Glaze SJ, Loudon M, Pitcher A *et al.* Aortic dilation in bicuspid aortic valve disease: flow pattern is a major contributor and differs with valve fusion type. *Circ Cardiovasc Imaging* 2013;**6**:499–507.
4. Erbel R, Aboyans V, Boileau C, Bossone E, Bartolomeo RD, Eggbrech H *et al.* ESC Guidelines on the diagnosis and treatment of aortic diseases. *Eur Heart J* 2014;**35**: 2873–926.
5. Vahanian A, Alfieri O, Andreotti F, Antunes MJ, Barón-Esquivias G, Baumgartner H *et al.* Guidelines on the management of valvular heart disease. *Eur Heart J* 2012;**33**: 2451–96.
6. Bieging ET, Frydrychowicz A, Wentland A, Landgraf BR, Johnson KM, Wieben O *et al.* In vivo three-dimensional MR wall shear stress estimation in ascending aortic dilatation. *J Magn Reson Imaging* 2011;**33**:589–97.
7. von Knobelsdorff-Brenkenhoff F, Rudolph A, Wassmuth R, Abdel-Aty H, Schulz-Menger J. Aortic dilatation in patients with prosthetic aortic valve: comparison of MRI and echocardiography. *J Heart Valve Dis* 2010;**19**:349–56.
8. Garcia J, Capoulade R, Le Ven F, Gaillard E, Kadem L, Pibarot P *et al.* Discrepancies between cardiovascular magnetic resonance and Doppler echocardiography in the measurement of transvalvular gradient in aortic stenosis: the effect of flow vorticity. *J Cardiovasc Magn Reson* 2013;**15**:84.
9. Sigovan M, Hope MD, Dyverfeldt P, Saloner D. Comparison of four-dimensional flow parameters for quantification of flow eccentricity in the ascending aorta. *J Magn Reson Imaging* 2011;**34**:1226–30.
10. Markl M, Harloff A, Bley TA, Zaitsev M, Jung B, Weigang E *et al.* Time-resolved 3D MR velocity mapping at 3T: improved navigator-gated assessment of vascular anatomy and blood flow. *J Magn Reson Imaging* 2007;**25**:824–31.
11. Sievers H-H, Stierle U, Mohamed SA, Hanke T, Richardt D, Schmidtke C *et al.* Toward individualized management of the ascending aorta in bicuspid aortic valve surgery: the role of valve phenotype in 1362 patients. *J Thorac Cardiovasc Surg* 2014; **148**:2072–80.
12. von Knobelsdorff-Brenkenhoff F, Gruettner H, Trauzeddel RF, Greiser A, Schulz-Menger J. Comparison of native high-resolution 3D and contrast-enhanced MR angiography for assessing the thoracic aorta. *Eur Heart J Cardiovasc Imaging* 2014;**15**:651–8.
13. Bock J, Kreher BW, Hennin J, Markl M. Optimized pre-processing of time-resolved 2D and 3D phase contrast MRI data. In: *15th Sci Meet Int Soc Magn Reson Med*, 2007. p. 3138.
14. Garcia J, Barker AJ, van Ooij P, Schnell S, Puthumana J, Bonow RO *et al.* Assessment of altered three-dimensional blood characteristics in aortic disease by velocity distribution analysis. *Magn Reson Med* 2015. doi:10.1002.mrm.25466.
15. Van Uitert R, Bitter I. Subvoxel precise skeletons of volumetric data based on fast marching methods. *Med Phys* 2007;**34**:627–38.
16. Garcia J, Marrufo OR, Rodriguez AO, Larose E, Pibarot P, Kadem L. Cardiovascular magnetic resonance evaluation of aortic stenosis severity using single plane measurement of effective orifice area. *J Cardiovasc Magn Reson* 2012;**14**:23.
17. Garcia J, Markl M, Schnell S, Allen B, Entezari P, Mahadevia R *et al.* Evaluation of aortic stenosis severity using 4D flow jet shear layer detection for the measurement of valve effective orifice area. *Magn Reson Imaging* 2014;**32**:891–8.
18. Cicchetti DV, Sparrow SA. Developing criteria for establishing interrater reliability of specific items: applications to assessment of adaptive behavior. *Am J Ment Defic* 1981;**86**:127–37.
19. Bock J, Frydrychowicz A, Stalder AF, Bley TA, Burkhardt H, Henning J *et al.* 4D phase contrast MRI at 3 T: effect of standard and blood-pool contrast agents on SNR, PC-MRA, and blood flow visualization. *Magn Reson Med* 2010;**63**:330–8.
20. Strecker C, Harloff A, Wallis W, Markl M. Flow-sensitive 4D MRI of the thoracic aorta: Comparison of image quality, quantitative flow, and wall parameters at 1.5T and 3T. *J Magn Reson Imaging* 2012;**36**:1097–103.
21. Barker AJ, Markl M, Bürk J, Lorenz R, Bock J, Bauer S *et al.* Bicuspid aortic valve is associated with altered wall shear stress in the ascending aorta. *Circ Cardiovasc Imaging* 2012;**5**:457–66.
22. Hope MD, Hope TA, Crook SE, Ordovas KG, Urbania TH, Alley MT *et al.* 4D flow CMR in assessment of valve-related ascending aortic disease. *JACC Cardiovasc Imaging* 2011;**4**:781–7.
23. Johnson KM, Lum DP, Turski PA, Block WF, Mistretta CA, Wieben O. Improved 3D phase contrast MRI with off-resonance corrected dual echo VIPR. *Magn Reson Med* 2008;**60**:1329–36.
24. Garcia D, Kadem L. What do we mean by aoritc valve area: geometric orifice area, effective orifice area, or gorlin area? *J Heart Valve Dis* 2006;**15**:601–8.
25. Meierhofer C, Schneider EP, Lyko C, Hutter A, Martinoff S, Markl M *et al.* Wall shear stress and flow patterns in the ascending aorta in patients with bicuspid aortic valves differ significantly from tricuspid aortic valves: a prospective study. *Eur Heart J Cardiovasc Imaging* 2013;**14**:797–804.
26. Verma S, Yanagawa B, Kalra S, Ruel M, Peterson MD, Yamashita MH *et al.* Knowledge, attitudes, and practice patterns in surgical management of bicuspid aortopathy: a survey of 100 cardiac surgeons. *J Thorac Cardiovasc Surg* 2013;**146**: 1033–1040.e4.
27. Leone O, Biagini E, Pacini D, Zagnoni S, Ferlito M, Graziosi M *et al.* The elusive link between aortic wall histology and echocardiographic anatomy in bicuspid aortic valve: implications for prophylactic surgery. *Eur J Cardiothorac Surg* 2012;**41**:322–7.
28. Della Corte A, Bancone C, Dialetto G, Covino FE, Manduca S, Montibello MV *et al.* The ascending aorta with bicuspid aortic valve: a phenotypic classification with potential prognostic significance. *Eur J Cardiothorac Surg* 2014;**46**:240–7.
29. Kang J-W, Song HG, Yang DH, Baek S, Kim D-H, Song JM *et al.* Association between bicuspid aortic valve phenotype and patterns of valvular dysfunction and bicuspid aortopathy. *JACC Cardiovasc Imaging* 2013;**6**:150–61.
30. Sievers H-H, Sievers HL. Aortopathy in bicuspid aortic valve disease - genes or hemodynamics? or Scylla and Charybdis? *Eur J Cardiothorac Surg* 2011;**39**:803–4.
31. Elefteriades JA, Farkas EA. Thoracic aortic aneurysm clinically pertinent controversies and uncertainties. *J Am Coll Cardiol* 2010;**55**:841–57.